S©MR ISSN 1813-3304

СИБИРСКИЕ ЭЛЕКТРОННЫЕ
МАТЕМАТИЧЕСКИЕ ИЗВЕСТИЯ

Siberian Electronic Mathematical Reports
http://semr.math.nsc.ru

Том 12, стр. 465–479 (2015) УДК 519.245
DOI 10.17377/semi.2015.12.040 MSC 65C20

STATISTICAL SIMULATION TECHNIQUE FOR DEFORMATION BAND SPATIAL DISTRIBUTION IN THE FAULT DAMAGE ZONE

D.R. KOLYUKHIN

Abstract. The paper presents two methods for statistical simulation of deformation bands distribution for reservoir modelling purposes based on analysis of field data. The proposed algorithms reproduce spatial density distribution and clustering of deformation bands observed in fault damage zones. Application and precision of the algorithms for different parameter values have been checked numerically.

Keywords: statistical simulation, fault damage zone, deformation bands, fractals and multifractals, correlation dimension.

1. Introduction

This paper addresses a method for statistical simulation of the spatial distribution of deformation bands in fault damage zones. Deformation bands, an intrinsic element of fault zones in porous rock, affect subsurface fluid flow by acting as barriers or baffles ([1], [11], [12], [21]). Forecasting deformation band distribution in sub-surface reservoirs has, therefore, significant value for petroleum exploration and production purposes, as well as for the evaluation of potential sites for CO2 sequestration.

The geometry and spatial distribution of deformation bands in fault zones resemble to a certain extent those of fractures, a topic of a number of previous studies.

Kolyukhin, D.R., Statistical simulation technique for deformation band spatial distribution in the fault damage zone.

The financial support from Statoil-VISTA programme, a research cooperation between the Norwegian Academy of Science and Letters and Statoil (VISTA Project 6348) and from RFBR (grant no. 14-05-93090 and 15-55-20004) is gratefully acknowledged. The author is grateful to Sylvie Schueller and Jan Tveranger for their constructive comments on an earlier version of the manuscript.

Received July, 3, 2015, published September, 9, 2015.

Statistical analysis of extensive fracture datasets was carried out by Odling et al. [17], [18]. Fractal and multifractal description ([3], [4], [7]) have been proposed for scaling of observed fracture systems. An unbiased method for multifractal analysis that takes into account the finite domain size and boundary effects was developed by Ouillon and Sornette [19].

Simulation of fracture networks for modelling purposes has been addressed by several authors ([8], [23]). A statistical model of fracture distribution in fault damage zone was presented by Harris et al. [15]. Belfield [2] used a multifractal model of strain distribution in rock masses to simulate the spatial distribution of the fractures.

Compared to the number of studies dedicated to fractures, less attention has been paid to the spatial distribution of deformation bands in fault damage zones. Statistical analysis of extensive datasets collected from outcrops has been carried out by Du Bernard et al. [9], Kolyukhin et al. [16], and Schueller et al. [22]. Their approaches resemble that used by Odling et al. [17], [18] for studying fracture networks.

The simulation of the spatial distribution of deformation bands is performed in [9], [16]. A deterministic statistical model for damage zone growth based on the deformation bands simulation is suggested in [22]. As well as in previous studies, the algorithms presented in this paper are based on using a multiplicative cascade technique described in [7]. The purpose of this study is to extend this approach and adapt a simulation algorithm for a more thorough use of available results of the statistical analysis. The simulation (or sampling) algorithm proposed here is based on the results of the statistical analysis of outcrop data presented by Schueller et al. [22].

At the end of Introduction I want to notice that modeling of spatial distribution of deformation bands plays the important role in the modeling of fault damage zone. In general a fault zone has very complex structure and consists of many structural elements [5]. In [24] it was proposed to employ the fault facies technique to overcome these difficulties. Suggested method allows to perform an explicit three-dimensional statistical simulation of fault damage zone. Further this approach was developed e.g. in [10], [20]. The key point of these models is a distribution of deformation bands estimated from analysis of outcrop data.

2. Statistical method

Here we consider a one-dimensional model of band density along a straight line starting at a fault core boundary and running perpendicular to the fault plane (or more precisely to the fault strike). The frequency of deformation bands decreases with distance from the fault [9]. The relationship between band frequency, fault throw and distance from the fault core was considered by Schueller et al. [22] who recognized a logarithmic decrease of band frequency at increasing distance from a fault

$$Y = A + L \ln x \tag{1}$$

where Y represents the frequency of deformation bands per meter and x the distance from the fault core. Then the probability density of band distribution is proportional to Y from (1) and has a form:

$$p(x) \propto 1 - B \ln x, \quad B = -\frac{L}{A}, \quad x \in [x_{min}, x_{max}]. \tag{2}$$

Here x, x_{min}, x_{max} have dimension meter (m), other variables are dimensionless. Model parameters B, x_{min}, x_{max} allow consideration of a wide range of logarithmically decreasing functions described in [16] and [22]. However, this relation alone does not capture the observed clustering of bands, described in [9], [16], [22], which is characterized by a multifractal correlation dimension.

Following [9], [22], the intersections of N_{db} deformation bands with scanline are considered in this work as a multifractal set $\Theta = \{X_1, \ldots, X_{N_{db}}\}$. Multifractals are generalizations of fractals. In general, their spatial distribution is characterized by the infinite multifractal spectrum [25]:

$$D_{-\infty} \geq \ldots \geq D_0 \geq D_1 \geq \ldots \geq D_{-\infty}.$$

The segment is covered by a regular grid of mesh size ϵ. $i-th$ cell is characterised by probability $p(\epsilon)$ that arbitrary deformation band $x_j, 1 \leq j \leq N_{db}$ falls in this cell. Multifractal dimensions can be defined as [19], [25]

$$D_q = \begin{cases} \frac{1}{q-1} \lim_{\epsilon \to 0} \frac{\sum_{i=1}^{N(\epsilon)} p_i^q(\epsilon)}{\ln \epsilon}, & q \neq 1 \\ \lim_{\epsilon \to 0} \frac{\sum_{i=1}^{N(\epsilon)} \ln p_i(\epsilon) p_i(\epsilon)}{\ln \epsilon}, & q = 1 \end{cases} \tag{3}$$

where $N(\epsilon)$ is the number of non-empty cells at scale ϵ.

D_2 is also called the correlation dimension and can be estimated by using (4), (5) suggested by Grassberger and Procaccia [14] and used in [9], [22].

$$C_2(r) = \lim_{N_{db} \to \infty} \frac{2}{N_{db}(N_{db}-1)} \sum_{i<j} \theta(r - |x_i - x_j|). \tag{4}$$

$$D_c = \lim_{r \to 0} \frac{\ln C_2(r)}{\ln r}. \tag{5}$$

Here, N_{db} is a total number of deformation bands, x is a band's position, r is a distance, $C_2(r)$ is a pair correlation function, $\theta(x)$ is the Heaviside function whose value is zero for a negative argument and one otherwise, D_c is an approximation of D_2. For D_c the values estimated in Du Bernard et al. [9] and Schueller et al. [22] are 0.87 ± 0.05 and 0.84 ± 0.06, respectively.

An iterative algorithm for simulation of random fields with multifractal probability density distribution is described by Darcel et al. [7]. The studied domain is divided into cells and a probability value corresponding to the frequency of deformation bands is assigned to each cell. At the start of any iteration, each subdomain dimension is divided into l equal parts. In Fig. 1 the isotropic fragmentation procedure is illustrated for first and second iterations with $l = 2$. If the probability of the original subdomain equals P, then the probabilities of the resulting subdomains are P_1P, P_2P in random order. The probabilities $P_1, \ldots, P_n$ are defined by the following equation:

$$\sum_{i=1}^{n} \frac{P_i^q}{(1/l)^{(q-1)D_q}} = 1. \tag{6}$$

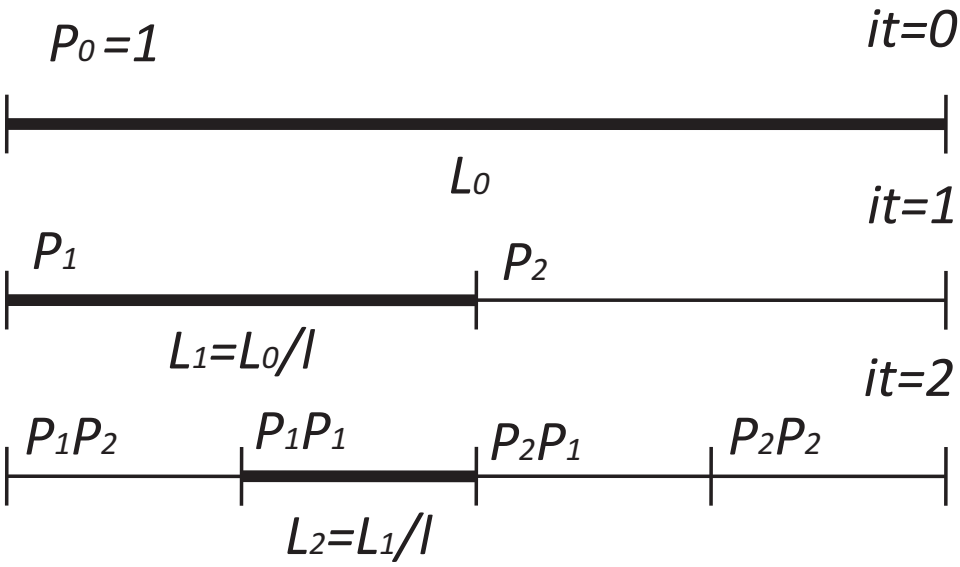

FIG. 1. The two first iterations of the general multifractal simulation scheme. Here $l = 2$.

Here we consider a one-dimensional case, therefore $n = l$.

Dependence of correlation dimensions estimated by (5) ($\hat{D}_c$) and (3) ($\hat{D}_2$) on true value of D_2 is presented in Fig. 2. Here, $N_{db} = 100$ deformation bands are generated by the method illustrated in Fig. 1. Probability $p_i(\epsilon)$ in (3) is estimated as a ratio of a number of deformation bands sampled in the $i - th$ cell to a total number of deformation bands N_{db}.

The aim of this work is to provide a method for statistical simulation (or sampling by Monte Carlo method) of band distributions with certain values of D_2. The iterative algorithm described above provides a means to do so. For $n = 2$, probabilities P_1 and P_2 are uniquely defined by (6). However, increasing n provides additional degrees of freedom that can be employed to approximate density $p(x)$ in (2). In this work $n = 4$. In the first suggested algorithm P_1, P_2, P_3, P_4 are calculated as a solution for the optimization problem defined by (7) as long as (6) is satisfied exactly.

$$\|\mathbf{F} - \mathbf{P}\| + \left((F_1 - P_1)^2 + (F_2 - P_2)^2 + (F_3 - P_3)^2 + (F_4 - P_4)^2\right)^{0.5} \to \min, \tag{7}$$

where x_i, x_{i+1} - the left and right borders of a corresponding cell at current iteration and

$$F_i(x) = \int_{x_i}^{x_{i+1}} p(x)dx.$$

Here and below a bold font is used for vectors.

Thus, the probability density function $F(x)$ is a stepwise approximation of $p(x)$. The fact that equation (6) holds in the process of modelling, ensures the adequate simulation of deformation bands clustering determined by a given value of D_2. However, it can be a problem to satisfy the condition described by (2) even for $n = 4$. To overcome this difficulty in the second algorithm an additional term is

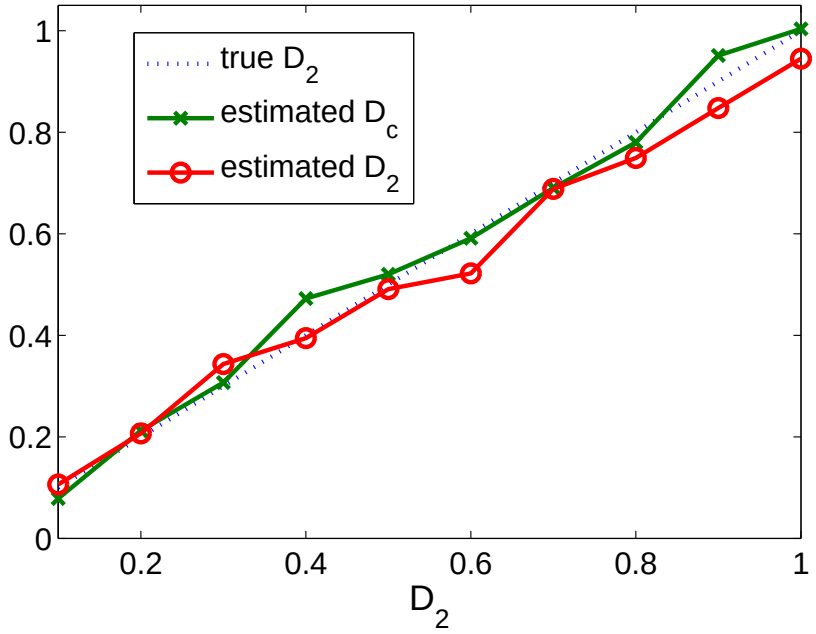

FIG. 2. Dependence of correlation dimensions estimated by (5) ($\hat{D}_c$) and (3) ($\hat{D}_2$) on true D_2.

involved in the minimizing function (8) in order to control the balance between the two main model requirements ($p(x)$ and D_2)

$$\|\mathbf{F}-\mathbf{P}\| + exp(-\alpha \cdot it^2) \left\| \sum_{i=1}^{4} P_i^2 - \left(\frac{1}{l}\right)^{D_2} \right\| \to \min \tag{8}$$

where it is an order number of current iteration.

The second algorithm (8) relaxes conditions defined by (6) in the first iterations which are the most important to satisfy (2). Here, α is a turning parameter which allows to control the balance between (2) and (6). The first iteration of a numerical procedure defined by (7) and (8) is illustrated in Fig. 3 for $D_2 = 0.6, B = 0.34, x_{min} = 0, x_{max} = 10m, \alpha = 0.1$. Probability density $p(x)$ defined by (2) compares with approximation defined by vector $\mathbf{P}$. Norm $\|\mathbf{F}-\mathbf{P}\|$ equals 0.17 and 0.002 for the first and second algorithms respectively. On the other hand, the corresponding values of ratio $\ln\left(\sum_{i=1}^{N(\epsilon)} p_i^2(\epsilon)\right)/\ln\epsilon$ which should tend to D_2 equal 0.6 and 0.83 (see Table 3). The comparison of corresponding algorithms is studied in the next section.

3. RESULTS

The results of the numerical testing of the first and second simulation methods (methods defined by (7) and (8) respectively) are presented in Figs. 4 and 5 and Figs. 6 and 7 respectively. The curves shown in Figs. 4 and 6 are sampled for

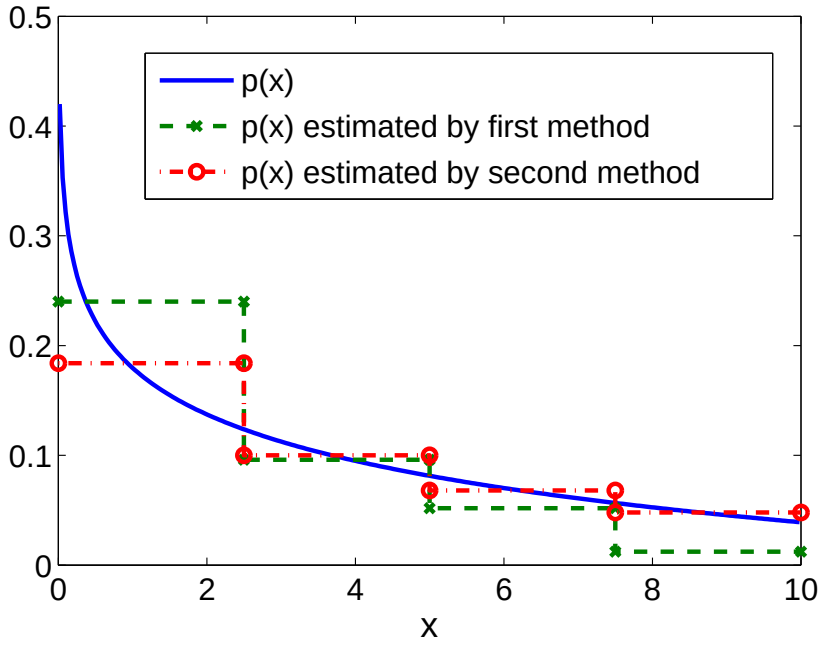

FIG. 3. Illustration of the first iteration of numerical procedure defined by (7) and (8). $D_2 = 0.6, B = 0.34, x_{min} = 0, x_{max} = 10m$.

$D_2 = 0.84$ obtained as result of the statistical analysis in [22]; those in Figs. 5 and 7 are sampled for $D_2 = 0.6$. Theoretical probability density $p(x)$ and the estimated density of sampled deformation bands are presented in Figs. 4a, 5a, 6a and 7a. Agreement between simulated data and theoretical density $p(x)$ is checked by using the Kolmogorov-Smirnov test. The pair correlation function $C_2(r)$ and its approximation are presented in Figs. 4b, 5b, 6b and 7b. Computations presented in Figs. 4-7 are performed for $B = 0.34$ obtained as a result of the statistical analysis in [22]. In each example presented in this section $N_{db} = 100, x_{min} = 0, x_{max} = 10m$, the number of iterations in the second method (8) is $T = 4$.

More detailed information about results of the statistical analysis of these and other computations is presented in Table 1. Numerical results of simulations are performed by using two developed methods ((7) and (8)) for different values of D_2. Statistical validation was performed by considering the corresponding $p - values$. The $p - value$ is the probability of obtaining the test statistic equal or more extreme than what was actually observed [13]. If the $p - value$ is less than the significance level, the null hypothesis is rejected. In all considered cases a $p - values$ of the samples simulated by using (8) are greater than a usually used significance level 0.05. Corresponding $p - values$ are estimated after the last $T - th$ iteration by using Kolmogorov-Smirnov test. Thus, the hypothesis claiming that simulated deformation bands are distributed according to probability density $p(x)$ is accepted. On the other hand, the same hypothesis should be rejected for the deformation bands sampled by using (7) for $D_2 = 0.6, 0.7$. This example shows that employment

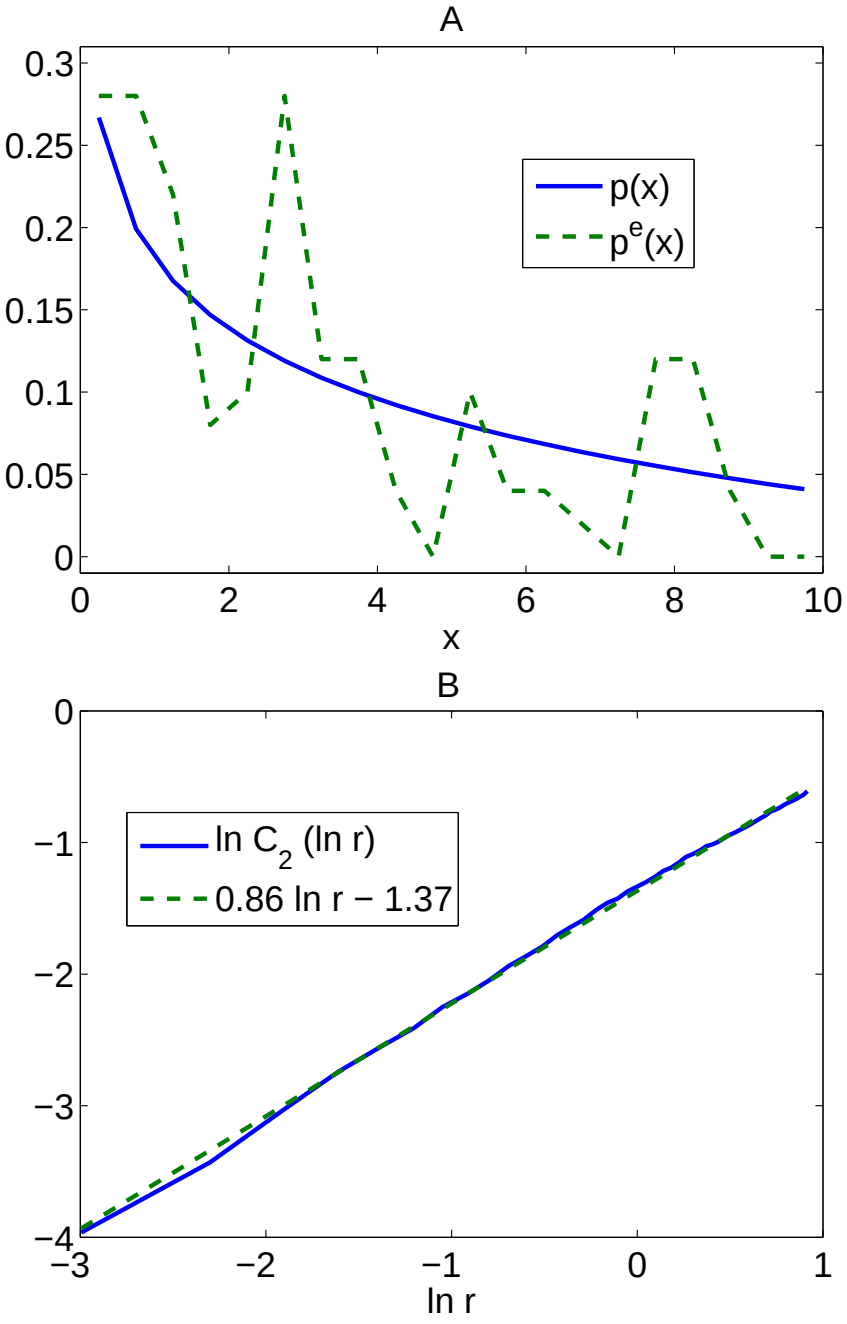

FIG. 4. (a) Theoretical (solid line) and estimated (dash line) density of deformation bands sampled by first method (7). Kolmogorov-Smirnov test $p - value = 0.11$. (b) Correlation function $C_2(x)$ and its approximation. $\hat{D}_c = 0.86, D_2 = 0.84, B = 0.34, x_{min} = 0, x_{max} = 10m$.

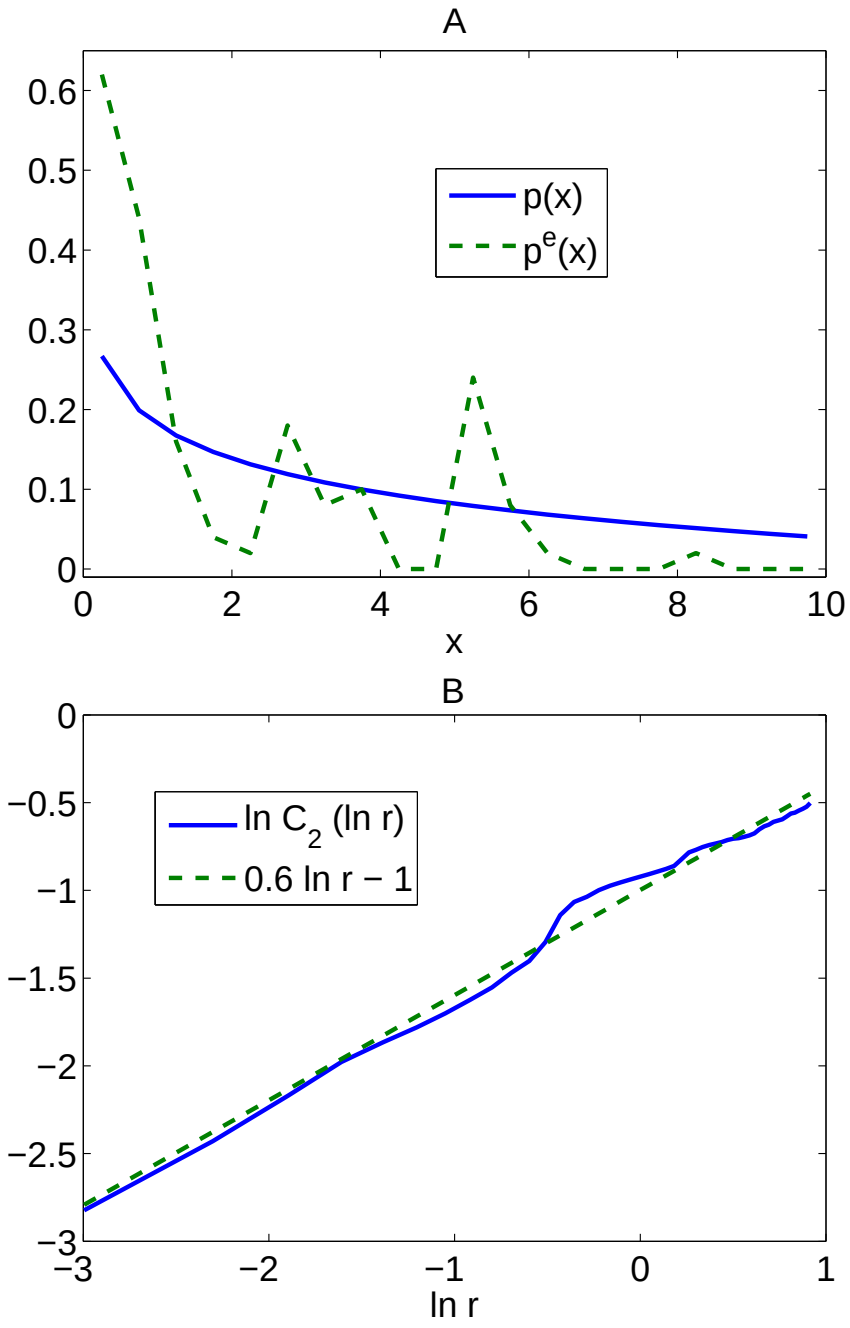

FIG. 5. (a) Theoretical (solid line) and estimated (dash line) density of deformation bands sampled by first method (7). Kolmogorov-Smirnov test $p - value = 3.1E - 9$. (b) Correlation function $C_2(x)$ and its approximation. $\hat{D_c} = 0.6, D_2 = 0.6, B = 0.34, x_{min} = 0, x_{max} = 10m$.

TABLE 1. Numerical results of simulations performed by using two developed methods (Eqs. (7) and (8))) for different values of D_2. $p-values$ estimated by using Kolmogorov-Smirnov test and correlation dimensions estimated by (5) ($\hat{D}_c$) and (3) ($\hat{D}_2$) are presented. $p-values$ of resulting $\hat{D}_2$ are estimated by using (9). $B = 0.34, x_{min} = 0, x_{max} = 10m$

Type of suggested method	True D_2	Kolmogorov-Smirnov test $p-value$	$\hat{D}_c$	$\hat{D}_2$ ($p-value$ estimated by using (9))
Eq. (7)	0.6	3.1E-9	0.6	0.58 (0.61)
Eq. (7)	0.7	1,88E-4	0.62	0.66 (0.51)
Eq. (7)	0.8	0.11	0.84	0.75 (0.64)
Eq. (7)	0.84	0.11	0.86	0.79 (0.76)
Eq. (7)	0.9	0.14	0.88	0.82 (0.60)
Eq. (8), $\alpha = 0.075$	0.6	0.09	0.69	0.58 (0.62)
Eq. (8), $\alpha = 0.15$	0.7	0.13	0.71	0.69 (0.84)
Eq. (8), $\alpha = 0.2$	0.8	0.25	0.84	0.81 (0.13)
Eq. (8), $\alpha = 0.2$	0.84	0.10	0.84	0.78 (0.67)
Eq. (8), $\alpha = 0.25$	0.9	0.13	0.87	0.82 (0.59)

of the first algorithm (7) can not ensure the fulfillment of the conditions defined by (1) and (2).

The correlation dimensions estimated by (5) ($\hat{D}_c$) and (3) ($\hat{D}_2$) are also presented in Table 1. An agreement between $\hat{D}_2$ and D_2 can be checked by using the bootstrap method [6]. For this purpose N_{bs} realizations of spatial distributions of deformation bands are generated by using an iterative cascade method [7] described in Section 2. For each realization i an approximation $\hat{D}_2^i$ is evaluated by (3). Then the corresponding $p-values$ can be estimated as fraction

$$p-value = \frac{\#\left\{|\hat{D}_2 - D_2| < |\hat{D}_2^i - D_2|\right\}}{N_{bs}}, \quad i = 1, \ldots, N_{bs}. \tag{9}$$

From Table 1 it is seen that the accuracy of estimation $\hat{D}_c$ is comparable with the accuracy of estimation $\hat{D}_2$ for which p-value calculated by using (9) is greater than significance value 0.05 for all considered cases for the both developed methods. In all computations performed in this section $N_{bs} = 10^4$. Note that in order to satisfy each of the conditions defined by (1) and (2) and the condition defined by (3) and (5) for different D_2 values different α values are used in the second method (8).

Accuracy of estimations $\hat{D}_c$ and $\hat{D}_2$ depends on implementation of (6) in the developed methods. In the first method (7) the conditions defined by (6) are satisfied automatically. In the second method (8) $\ln\left(\sum_{i=1}^{N(\epsilon)} p_i^2(\epsilon)\right)/\ln\epsilon$ can differ significantly from required D_2 in the first iterations (corresponding dependencies are presented in Tables 2 and 3). However, in the last iterations these values are practically equal.

The dependence of simulation results on parameter B is illustrated in Tables 4 and 5 for $D_2 = 0.84$ and $D_2 = 0.6$ respectively. $p-values$ estimated by using Kolmogorov-Smirnov test and correlation dimensions estimated by (5) ($\hat{D}_c$) and

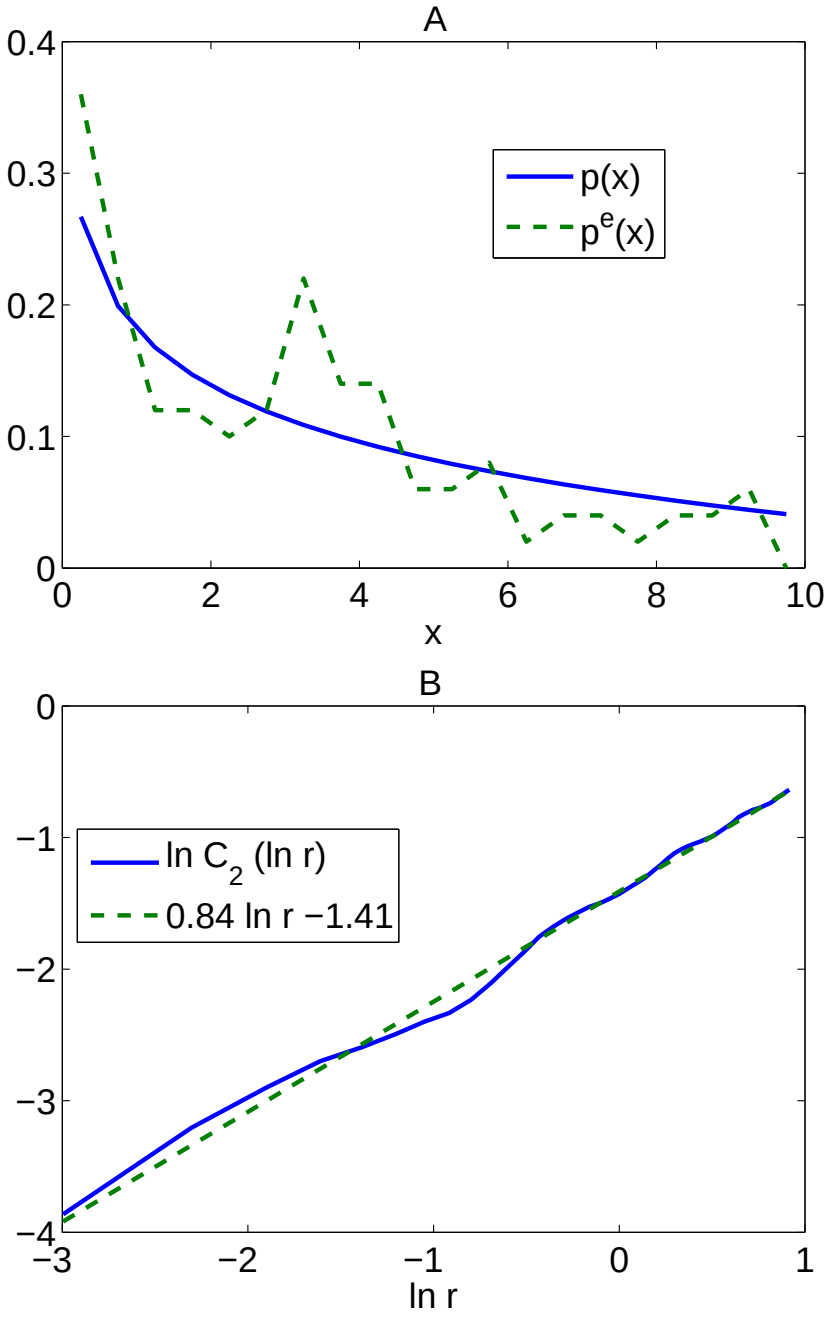

FIG. 6. (a) Theoretical (solid line) and estimated (dash line) density of deformation bands sampled by first method (8). Kolmogorov-Smirnov test $p-value = 0.1$. (b) Correlation function $C_2(x)$ and its approximation. $\hat{D}_c = 0.84, D_2 = 0.84, B = 0.34, x_{min} = 0, x_{max} = 10m, \alpha = 0.2$.

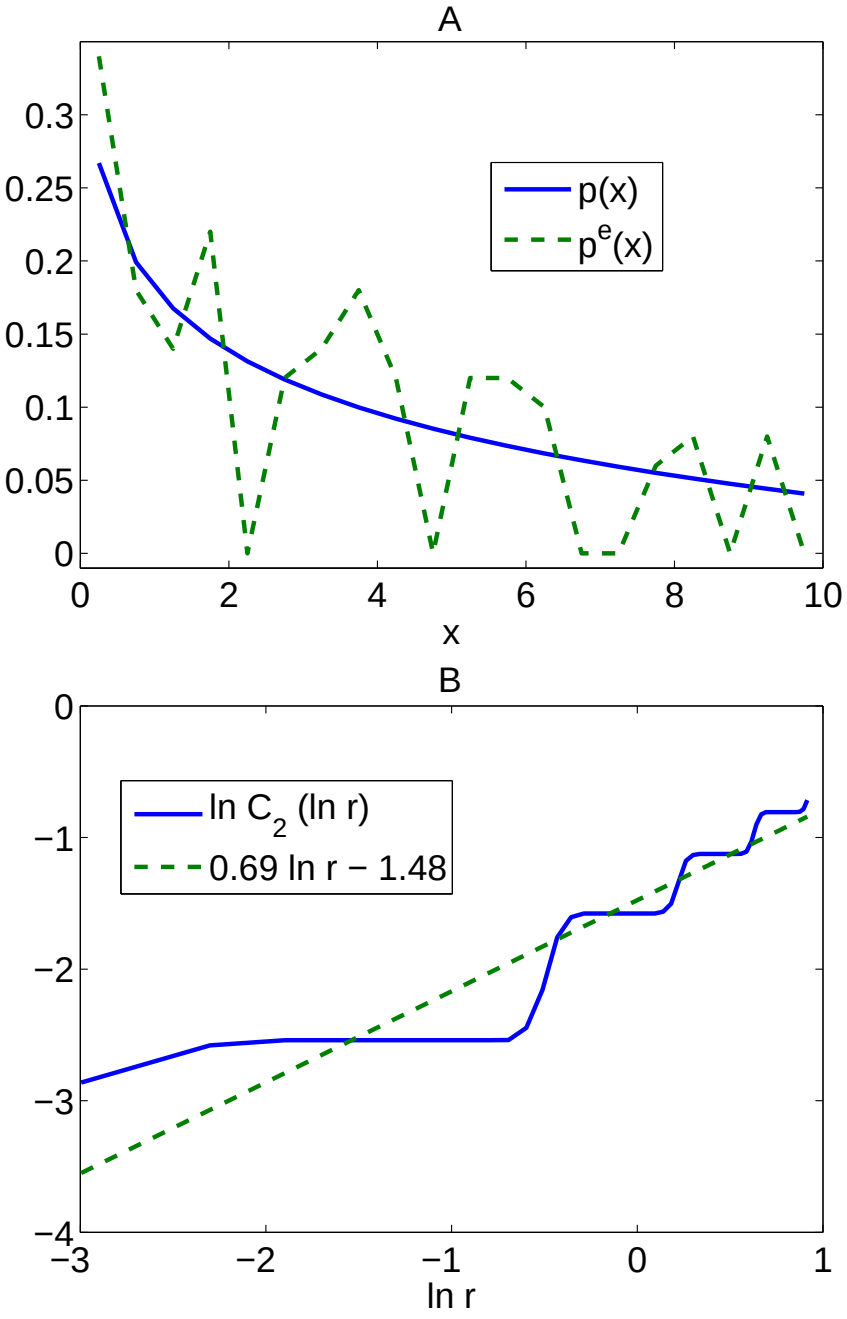

FIG. 7. (a) Theoretical (solid line) and estimated (dash line) density of deformation bands sampled by first method (8). Kolmogorov-Smirnov test $p - value = 0.09$. (b) Correlation function $C_2(x)$ and its approximation. $\hat{D}_c = 0.69, D_2 = 0.6, B = 0.34, x_{min} = 0, x_{max} = 10m, \alpha = 0.075$.

TABLE 2. Dependence of correlation dimension estimated by using (3) on iteration number for the second simulation method (8). $D_2 = 0.84, B = 0.34, x_{min} = 0, x_{max} = 10m$

Iteration	$\ln\left(\sum_{i=1}^{N(\epsilon)} p_i^2(\epsilon)\right)/\ln\epsilon$
1	0.83
2	0.89
3	0.84
4	0.84

TABLE 3. Dependence of correlation dimension estimated by using (3) on iteration number for the second simulation method (8). $D_2 = 0.6, B = 0.34, x_{min} = 0, x_{max} = 10m$

Iteration	$\ln\left(\sum_{i=1}^{N(\epsilon)} p_i^2(\epsilon)\right)/\ln\epsilon$
1	0.83
2	0.89
3	0.6
4	0.6

TABLE 4. Numerical results of simulations performed by using two developed methods (Eqs. (7) and (8)) for different values of B. $p-values$ estimated by using Kolmogorov-Smirnov test and correlation dimensions estimated by (5) ($\hat{D}_c$) and (3) ($\hat{D}_2$) are presented. $p-values$ of resulting $\hat{D}_2$ are estimated by using (9). $D = 0.84, x_{min} = 0, x_{max} = 10m$

Type of suggested method	B	Kolmogorov-Smirnov test $p-value$	$\hat{D}_c$	$\hat{D}_2$ ($p-value$ estimated by using (9))
Eq. (7)	0.2	0.0062	0.85	0.82 (0.98)
Eq. (7)	0.3	0.27	0.8	0.79 (0.80)
Eq. (7)	0.43	0.10	0.85	0.75 (0.28)
Eq. (8), $\alpha = 0.075$	0.2	0.16	0.8	0.76 (0.41)
Eq. (8), $\alpha = 0.075$	0.3	0.68	0.88	0.82 (0.95)
Eq. (8), $\alpha = 0.075$	0.43	0.6	0.87	0.78 (0.66)

(3) ($\hat{D}_2$) are presented. $p-values$ of resulting $\hat{D}_2$ are estimated by using (9). From Table 5 it is seen that in case of small D_2 value the first method can not satisfy the agreement between sampled data and theoretical density ((1) and (2)) for any values of B. Moreover, as it is clear from Table 4 that for the first method this condition is also not satisfied for small values of B. On the other hand, in all considered cases it is possible to choose the value of parameter α which allows to perform statistical simulations fulfilling all required conditions.

Note that estimation of $p-values$ for Kolmogorov-Smirnov test and Eq. (9) allows to check the quality of sampled realizations and chose best of them. This approach was used to acheive sufficiently accurate results presented in this section.

TABLE 5. Numerical results of simulations performed by using two developed methods (Eqs. (7) and (8)) for different values of B. $p-values$ estimated by using Kolmogorov-Smirnov test and correlation dimensions estimated by (5) ($\hat{D}_c$) and (3) ($\hat{D}_2$) are presented. $p-values$ of resulting $\hat{D}_2$ are estimated by using (9). $D = 0.6, x_{min} = 0, x_{max} = 10m$

Type of suggested method	B	Kolmogorov-Smirnov test $p-value$	$\hat{D}_c$	$\hat{D}_2$ ($p-value$ estimated by using (9))
Eq. (7)	0.2	7.31e-010	0.67	0.63 (0.48)
Eq. (7)	0.3	1.83e-007	0.61	0.61 (0.85)
Eq. (7)	0.43	3.24e-007	0.53	0.54 (0.22)
Eq. (8) $\alpha = 0.05$	0.2	0.59	0.74	0.59 (0.76)
Eq. (8) $\alpha = 0.05$	0.3	0.16	0.70	0.57 (0.56)
Eq. (8) $\alpha = 0.075$	0.43	0.22	0.71	0.55 (0.32)

4. Conclusions

Two methods for statistically simulating the distribution of deformation bands are presented. Suggested algorithms are based on statistical analysis of field data by Schueller et al. [22]. Both of them are extension of a simulation technique described in [7] which has been used, for instance, in [9], [22]. The proposed approach captures key features of deformation band distributions in fault damage zones such as a decrease in deformation band frequency with increasing distance from the fault core and clustering of bands governed by multifractal correlation dimension D_2. The fulfillment of these two conditions is compared for both developed methods defined by (7) and (8). Numerical tests show that the second condition ((3) and (5)) is satisfied with sufficiently high accuracy for both methods, whereas the first condition ((1) and (2)) is not satisfied for the first method for small values of D_2 and B. In turn the right choice of the parameter alpha allows to satisfy this condition for the second method in all considered cases.

In this paper we consider D_2 only, but the suggested approach can be extended to incorporate several required multifractal dimensions D_i. Lower and upper bounds of fractal characteristics in nature [3] can also be taken into account. Developed methods can be also generalised on 2D or 3D cases.

References

[1] Antonellini M., Cilona A., Tondi E., Zambrano M., Agosta F., *Fluid flow numerical experiments of faulted porous carbonates, Northwest Sicily (Italy)*, Marine and Petrol. Geol. 55:186-201, 2014. doi:10.1016/j.marpetgeo.2013.12.003.

[2] Belfield W.C., *Incorporating spatial distribution into stochastic modelling of fractures: multifractals and Levy-stable statistics*, J. Struct. Geol. 20:473-486, 1998. doi: 10.1016/S0191-8141(97)00118-1S.

[3] Bonnet E, Bour O, Odling NE, Davy P, Main I, Cowie P, Berkowitz B., *Scaling of fracture systems in geological media*, Rev. Geophys. 39(3):347-383, 2001. doi:10.1029/1999RG000074.

[4] Bour O., Davy P., Darcel C., *A statistical scaling model for fracture network geometry, with validation on multiscale mapping of a joint network (Hornelen Basin, Norway)*, J. Geophys. Res. 107:B6, 2002. doi:10.1029/2001JB000176.

[5] Braathen, A., Tveranger, J., Fossen, H., Skar, T., Cardozo, N., Semshaug, S.E., Bastesen, E. and Sverdrup, E., *Fault facies and its application to sandstone reservoirs*, AAPG Bulletin 93:891-917, 2009. doi:10.1306/03230908116.

[6] Clauset A., Shalizi C.R., Newman M.E.J., *Power-law distributions in empirical data*, SIAM Review 51(4):661-703, 2009. doi:10.1137/070710111. MR2563829

[7] Darcel C., Bour O., Davy P., de Dreuzy J.R., *Connectivity properties of two-dimensional fracture network with stochastic fractal correlation*, Water Resources Res. 39(10):1272, 2003. doi:10.1029/2002WR001628.

[8] Dowd P.A., Xu C., Mardia K.V., Fowell R.J., *A Comparison of Method for the Stochastic Simulation of Rock Fractures*, Math. Geol. 39:697-714, 2007. doi:10.1007/s11004-007-9116-6.

[9] Du Bernard X., Labaume P., Darcel C., Davy P., Bour O., *Cataclastic slip band distribution in normal fault damage zones, Nubian sandstones, Suez rift*, J. Geophys. Res. 107:B7, 2002. doi:10.1029/2001JB000493.

[10] Fachri, M., Tveranger, J., Braathen, A., Schueller, S., *Sensitivity of fluid flow to deformation-band damage zone heterogeneities: A study using fault facies and truncated Gaussian simulation*, J. Struct. Geol. 52:60-79, 2013. doi:10.1016/j.jsg.2013.04.005.

[11] Fossen H., Bale A., *Deformation bands and their influence on fluid flow*, AAPG Bulletin 91(12):1685-1700, 2007. doi:10.1306/07300706146.

[12] Fossen H, Schultz R.A., Shipton Z.K., Mair K., *Deformation bands in sandstone: a review*, J. Geol. Soc., London 164:755-769, 2007. doi:10.1144/0016-76492006-036.

[13] Gelman A., *Commentary: P Values and Statistical Practice*, Epidemiology 24(1):69-72, 2013. doi:10.1097/EDE.0b013e31827886f7.

[14] Grassberger P., Procaccia I., *Measuring the strangeness of strange attractors*, Physica D: Nonlinear Phenomena 9(1-2):189-208, 1983. doi:10.1016/0167-2789(83)90298-1. MR0732572

[15] Harris S.D., McAllister E., Knipe R.J., Odling N.E., *Predicting the three-dimensional population characteristics of fault zones: a study using stochastic models*, J. Struct. Geol. 25(8):1281-1299, 2003. doi:10.1016/S0191-8141(02)00158-X.

[16] Kolyukhin D., Schueller S., Espedal M., Fossen H., *Deformation band populations in fault damage zone - impact on fluid flow*, Computational Geosciences 14(2):231-248, 2010. doi:10.1007/s10596-009-9148-8.

[17] Odling N.E., Gillespie P.A., Bourgine B., Castaing C., Chiles J.P., Christiansen N.P., Fillion E., Genter A., Olsen C., Thrane L., Trice R., Aarseth E., Walsh J.J., Watterson J., *Variations in fracture system geometry and their implications for fluid flow in fractured hydrocarbon reservoirs*, Petrol. Geosci. 5:373-384, 1999. doi:10.1144/petgeo.5.4.373.

[18] Odling N.E., *The scaling of hydrailic connectivity of in rock fracture zones*, Geophys. Res. Lett. 28(15):3019-3022, 2001. doi:0.1029/2000GL011863.

[19] Ouillon G., Sornette D., *Unbiased multifractal analysis: Application to fault patterns*, Geophys. Res. Lett. 23(23):3409-3412, 2001. doi:10.1029/96GL02379.

[20] Qu, D., Rиe, P., Tveranger, J., *A method for generating volumetric fault zone grids for pillar gridded reservoir models*, Computers and Geosciences 81:28–37, 2015. doi:10.1016/j.cageo.2015.04.009.

[21] Rotevatn A., Sandve T.H., Keilegavlen E., Kolyukhin D., Fossen H., *Deformation bands and their impact on fluid flow in sandstone reservoirs: the role of natural thickness variations*, Geofuids 13(3):359-371, 2013. doi:10.1111/gfl.12030.

[22] Schueller S., Braathen A., Fossen H., Tveranger J., *Spatial distribution of deformation bands in damage zones of extensional faults in porous sandstones: Statistical analysis of field data*, J. Struct. Geol. 52:148-162, 2013. doi:10.1016/j.jsg.2013.03.013.

[23] Tran N.H., *Simulated annealing technique in discrete fracture network inversion: optimizing the optimization*, Computational Geosciences 11:249-260, 2007. doi:10.1007/s10596-007-9049-7.

[24] Tveranger, J., Skar, T. Braathen A., *Incorporation of fault zones as volumes in reservoir models*, Bolletino di Geofisica Teorica e Applicata 45(1):316–318, 2004.

[25] Xie H., Wang J.A., Kwasniewski M.A., *Multifractal characterization of rock fracture surfaces*, Int. J. Rock. Mech. Min. Sci. 36:19-27, 1999. doi:10.1016/S0148-9062(98)00172-7.

Dmitriy Romanovich Kolyukhin
Uni Research CIPR,
Allegaten 41,
5007 Bergen, Norway
Present address:
Trofimuk Institute of Petroleum Geology and Geophysics SB RAS,
pr. Koptyuga, 3,
630090, Novosibirsk, Russia
E-mail address: KolyukhinDR@ipgg.sbras.ru